Research Square

Preprints are preliminary reports that have not undergone peer review.
They should not be considered conclusive, used to inform clinical practice,
or referenced by the media as validated information.

Inflammasome activation promotes the progression of myelodysplastic syndrome

Atsushi Iwama

03aiwama@ims.u-tokyo.ac.jp

The Institute of Medical Science, The University of Tokyo https://orcid.org/0000-0001-9410-8992

Shohei Andoh

The Institute of Medical Science, The University of Tokyo https://orcid.org/0000-0002-2746-1793

Yaeko Nakajima-Takagi

The Institute of Medical Science, The University of Tokyo, Tokyo

Shun Uemura

The University of Tokyo https://orcid.org/0000-0002-1520-6808

Yuya Atsuta

The Institute of Medical Science, The University of Tokyo

Takanori Fukuta

The University of Tokyo https://orcid.org/0000-0001-7852-1808

Makiko Miyota

The University of Tokyo

Akiho Tsuchiya

The University of Tokyo

Shuhei Koide

The Institute of Medical Science, The University of Tokyo

Motohiko Oshima

The Institute of Medical Science, The University of Tokyo

Bahityar Rahmutulla

Graduate School of Medicine, Chiba University

Atsushi Kaneda

Chiba University Graduate School of Medicine https://orcid.org/0000-0002-6980-5515

Shun'ichiro Taniguchi

Kagoshima University Graduate School of Medical and Dental Sciences

Takuro Nakamura

Tokyo Medical University https://orcid.org/0000-0002-0419-7547

Yasuhito Nannya

The Institute of Medical Science, The University of Tokyo https://orcid.org/0000-0002-6526-0992

Yoshihiro Hayashi

Ritsumeikan University

Hironori Harada

Tokyo University of Pharmacy and Life Sciences https://orcid.org/0000-0001-9401-5470

Article

Keywords:

Posted Date: September 3rd, 2026

DOI: https://doi.org/10.21203/rs.3.rs-10748625/v1

License: This work is licensed under a Creative Commons Attribution 4.0 International License.
Read Full License

Additional Declarations: There is **NO** conflict of interest to disclose.

Inflammasome activation promotes the progression of myelodysplastic syndrome

Shohei Andoh[1*], Yaeko Nakajima-Takagi[1*], Shun Uemura[1], Yuya Atsuta[1], Takanori Fukuta[1], Makiko Miyota[1], Akiho Saiki-Tsuchiya[1], Shuhei Koide[1], Motohiko Oshima[1], Bahityar Rahmutulla[2], Atsushi Kaneda[2,3], Shun'ichiro Taniguchi[4], Takuro Nakamura[5], Yasuhito Nannya[6], Yoshihiro Hayashi[7,8], Hironori Harada[7], and Atsushi Iwama[1,9]

[1] Division of Stem Cell and Molecular Medicine, Center for Stem Cell Biology and Regenerative Medicine, The Institute of Medical Science, The University of Tokyo, Tokyo, Japan.

[2] Department of Molecular Oncology, Graduate School of Medicine, Chiba University, Chiba, Japan

[3] Health and Disease Omics Center, Chiba University, Chiba, Japan.

[4] Advanced Cancer Medicine for Gynecologic Cancer, Kagoshima University Graduate School of Medical and Dental Sciences, Kagoshima, Japan.

[5] Department of Experimental Pathology, Institute of Medical Science, Tokyo Medical University, Tokyo, Japan.

[6] Division of Hematopoietic Disease Control, Institute of Medical Science, The University of Tokyo, Tokyo, Japan.

[7] School of Life Science, Tokyo University of Pharmacy and Life Sciences, Tokyo, Japan.

[8] Laboratory of Cancer Pathobiology and Therapeutics, College of Pharmaceutical Sciences, Ritsumeikan University, Shiga, Japan.

[9] Laboratory of Cellular and Molecular Chemistry, Graduate School of Pharmaceutical Sciences, The University of Tokyo, Tokyo, Japan.

*Co-first author

Correspondence: Atsushi Iwama, M.D., Ph.D.
Division of Stem Cell and Molecular Medicine, Center for Stem Cell Biology and Regenerative Medicine, Institute of Medical Science, The University of Tokyo
4-6-1 Shirokanedai, Minato-ku, Tokyo, 108-8639 Japan
Phone: +81-3-6409-2180, Fax: +81-3-6409-2182
E-mail: 03aiwama@ims.u-tokyo.ac.jp

Abstract

Inflammasomes are multiprotein complexes that sense pathogen- and damage-associated molecular patterns and induce inflammatory responses and have been implicated in the pathogenesis of myelodysplastic syndrome (MDS). However, their functional contribution to MDS progression *in vivo* have not yet been elucidated. Here, we investigated the effects of inflammasome inhibition in mouse models of MDS by deleting *Asc*, an adaptor protein that links inflammasome sensor proteins to caspase-1. *Asc*-deficient mice showed no significant hematopoietic defects under steady-state conditions or in competitive bone marrow reconstitution assays. In an MDS mouse model co-expressing $CBL^{\Delta E8/9}$ and $RUNX1^{S291fs}$, mice developed MDS and eventually progressed to acute myeloid leukemia regardless of *Asc* status. However, compared with wild-type MDS mice, which progressed to lethal MDS, *Asc*-deficient MDS mice exhibited attenuated caspase-1 activation, delayed MDS progression, and significantly prolonged survival. *Asc* deficiency also substantially attenuated the MDS phenotypes induced by *Tet2* deficiency. Levels of IL-1β and/or IL-18, key inflammatory cytokines produced downstream of inflammasome activation, were elevated in the bone marrow fluid of these MDS models and reduced by *Asc* deficiency. These findings demonstrate that ASC-dependent inflammasome signaling contributes to MDS progression *in vivo* and suggest that targeting inflammasome signaling may represent a potential therapeutic approach for MDS.

Introduction

Myelodysplastic syndrome (MDS) is a clonal hematopoietic stem cell disorder characterized by cytopenia due to enhanced apoptotic cell death and dysplasia in single or multiple blood cell lineages that eventually evolve into acute myeloid leukemia (AML) at high frequencies. Hematopoietic stem cell (HSC) transplantation is the only treatment to cure MDS. However, transplantation therapy in older adult patients with MDS is often difficult because of therapeutic toxicity[1]. Therefore, patients with MDS are treated according to disease type and risk classification based on a prognostic scoring system[2]. Some cases of MDS benefit from therapeutic agents such as azacitidine, a DNA methylation inhibitor, and lenalidomide, an immunomodulator, but eventually become refractory[3, 4] This underlines the need for further understanding of its pathogenesis and the emergence of new treatment options.

Inflammasomes are protein complexes that initiate the processing of inflammatory proteins and play a role in activating inflammatory responses by producing inflammatory cytokines during innate immune system responses[5, 6]. For example, NLRP3, a type of pattern recognition receptor, is activated when it encounters a pathogen or stress signal and recruits and binds to other molecules, such as apoptosis-associated speck-like protein containing a CARD (ASC) and caspase-1, to form an inflammasome complex. The inflammasome complex activates caspase-1, which converts inflammatory cytokines such as interleukin-1β (IL-1β) and IL-18 into their active forms. Moreover, activated caspase-1 also cleaves and activates gasdermin D. Activated gasdermin D forms a pore by disrupting the plasma membrane and causing an influx from the outside to the inside of the cell, resulting in cell swelling and cell death (pyroptosis). These pores also release active forms of IL-1β and IL-18, which elicit an immune response and mobilize immune cells to the site of infection or injury. Furthermore, it has been shown that plasma membrane disruption by gasdermin D can be reversible, allowing active IL-1β and IL-18 to be released without cell death[7].

77 Activation of the innate immune system is well known in MDS, where pattern recognition
78 receptors, such as toll-like receptors (TLRs), are activated by pathogen-associated molecular
79 patterns and host cell-derived damage-associated molecular patterns (DAMPs). Somatic gene
80 mutations in epigenetic modifiers, such as *TET2*, *DNMT3A*, *ASXL1*, *EZH2,* and spliceosomes,
81 are known to activate the innate immune system through various pathways[8]. Therefore, the
82 innate immune system is activated both endogenously and exogenously. Consequently,
83 inflammasome activation has also been implicated in MDS[8, 9]. Analyses of human MDS
84 samples have revealed that NLRP3 complexes activate caspase-1 in hematopoietic stem and
85 progenitor cells (HSPCs), promoting IL-1β and IL-18 production and inducing cell death[10, 11]
86 and that interventions in this pathway may ameliorate the ineffective hematopoiesis[10]. The
87 ASC adaptor protein is polymerized during inflammasome formation to form large filament-
88 like clusters called ASC specks, which are released during cell lysis. The average percentage
89 of ASC specks detected in the peripheral blood (PB) of MDS patients, particularly low-risk
90 MDS patients, was significantly higher than that in healthy individuals and patients with other
91 hematopoietic tumors, suggesting that it may be useful as a biomarker of MDS[12]. However,
92 the pathogenic significance of inflammasome activation in MDS progression has not been
93 elucidated using MDS mouse models *in vivo*.
94 *RUNX1* is a transcription factor that plays a variety of roles in hematopoiesis, including the
95 development of HSCs from the hemogenic endothelium and the differentiation and function
96 of hematopoietic cells. *RUNX1* mutations are found in ~10–20% of human MDS cases and
97 are known to contribute to the pathogenesis of MDS[13]. *CBL* is an E3 ubiquitin ligase that
98 negatively regulates intracellular signaling. *CBL* mutations are found in about 5–9% of
99 myeloid malignancies, including MDS[14], resulting in loss of ubiquitin activity and leading to
100 enhanced proliferative activity associated with increased tyrosine kinase activity. *RUNX1* and
101 *CBL* mutations co-occur at significant frequencies in MDS[15]. The mouse model of MDS

harboring *RUNX1*^{S291fs} mutant has been widely used[16]. Moreover, *CBL*^{Q367P} knock-in mice have been shown to develop chronic myelomonocytic leukemia[17]. Recently, a mouse model expressing *RUNX1*^{S291fs} combined with the deletion of *CBL* exon 8/9 (*CBL*$^{\Delta E8/9}$) was shown to reproduce the phenotypes characteristic of MDS with a short latency[18]. In this study, we aimed to elucidate the pathogenic significance of inflammasome activation in the progression of MDS using *Asc*-deficient *RUNX1*^{S291fs}*CBL*$^{\Delta E8/9}$ MDS mice.

Materials and Methods

Mice

The CD45.1^{+} mice used as recipients for transplantation experiments were purchased from Sankyo Labo Service Corporation, Inc. All experiments using mice were performed in accordance with our institutional guidelines for the use of laboratory animals and were approved by the Review Board for Animal Experiments and Recombinant DNA Experiments of the University of Tokyo (approval ID: PA22-17 and K23-465). *Asc*$^{-/-}$, *Vav1-iCre, and Tet2*$^{fl/fl}$ mice have been previously described[19-21]. *Asc*$^{+/-}$ mice were crossed to obtain *Asc*$^{-/-}$ mice. The following primers were used for genotyping:

Asc WT 5′-primer/ CCAGGTAATGGTTAATCCCAGCAACC

Asc LacZ 5′-primer/ GTAGGGGTTTTTCACAGACCGCTTTC

Asc 3′-primer/ TTGGCATTGCATGACATGGTGCACAC

Vav-iCre Tg F-primer/ GGTGTTGTAGTTGTCCCCACT

Vav1-iCre Tg R-primer/ CAGGTTTTGGTGCACAGTCA

Tet2 flox F-primer/ ATGAACCGAGAGTCCCTG TT

Tet2 flox R-primer/ TTCTTTAGCCCTTGCTGAGC

Flow cytometric analysis and antibodies

All flow cytometric analyses and cell sorting were performed using a FACSCelesta or FACSAria IIIu (BD Biosciences). Data were analyzed using FlowJo v10.6.1. Monoclonal antibodies recognizing the following antigens were used in flow cytometry and cell sorting: CD45.2 (104), CD45.1 (A20), Gr-1 (RB6-8C5), CD11b/Mac-1 (M1/70), Ter-119 (TER119), CD71 (RI7217), CD150 (TC15-12F12.2), CD34 (RAM34), CD48(HM48-1), CD135(A2F10), CD127/IL-7R (A7R34), B220 (RA3-6B2), CD117/c-kit (2B8), Sca-1 (D7), CD16/32/FcγRII-III (93), CD4 (GK1.5), CD8 (53-6.7), CD44 (IM7), CD115 (AFS98),

Ly6G (1A8) and lineage mixture (Gr-1, CD11b/Mac-1, Ter-119, CD127/IL-7R, B220, CD4, CD8α). The antibodies were purchased from BioLegend, eBioScience, or BD Biosciences. Dead cells were eliminated by staining with 1 μg/ml propidium iodide (Sigma-Aldrich). The cell surface protein expression used to identify hematopoietic cell types was as follows.

HSC (hematopoietic stem cell): $CD150^{+}CD48^{-}CD135^{-}CD34^{-}$c-$kit^{+}Sca\text{-}1^{+}Lineage^{-}$

CMP (common myeloid progenitor): $CD34^{+}Fc\gamma R^{-}$c-$kit^{+}Sca\text{-}1^{-}Lineage^{-}$

GMP (granulocyte-macrophage progenitor): $CD34^{+}Fc\gamma R^{+}$c-$kit^{+}Sca\text{-}1^{-}Lineage^{-}$

MEP (megakaryocyte-erythroblast progenitor): $CD34^{-}Fc\gamma R^{-}$c-$kit^{+}Sca\text{-}1^{-}Lineage^{-}$

LSK (hematopoietic stem and progenitor cells): c-$kit^{+}Sca\text{-}1^{+}Lineage^{-}$

LK (hematopoietic progenitor cells): c-$kit^{+}Lineage^{-}$

Myeloid cell: Mac-1^{+} and/or Gr-1^{+}

B cell: $B220^{+}$

T cell: $CD4^{+}$ and/or $CD8a^{+}$

Monocytes: Mac-$1^{+}CD115^{+}Ly6G^{-}$

Neutrophils: Mac-$1^{+}Ly6G^{+}$

$CBL^{\Delta E8/9}RUNX1^{S291fs}$ cell culture and MDS mouse model

According to the previous report[18], Platinum-E cells were transfected with pMY-IRES-hNGFR-*RUNX1S291fs* and pMY-IRES-GFP-$CBL^{\Delta E8/9}$ retroviral vectors using FuGENE HD Reagent (Promega). The medium was replaced 20 h after transfection, and the supernatant containing the retroviruses was collected and concentrated using a Retro-X Concentrator (Takara). c-kit positive cells from WT and $Asc^{-/-}$ mice were isolated by MACS columns (Miltenyi Biotec) and cultured in IMDM supplemented with 20% FBS, 1% penicillin/streptomycin/glutamine, stem cell factor (SCF) (50 ng/mL), thrombopoietin (TPO) (50 ng/mL), Flt3L (50 ng/mL), and IL-6 (50 ng/mL) for 24 h. The cells were transduced with

158 retroviruses for 72 h using RetroNectin (Takara Bio). For *in vitro* culture, $Lin^{-}hNGFR^{+}GFP^{+}$
159 cells were sorted using a FACSAria IIIu (BD) and cultured in IMDM supplemented with 20%
160 FBS, 1% penicillin/streptomycin/glutamine, SCF (50 ng/mL), TPO (50 ng/mL), IL-3 (20
161 ng/mL), and granulocyte-macrophage colony-stimulating factor (GM-CSF) (20 ng/mL).
162 Viable cells in the culture were counted using a Vi-CELL (Beckman Coulter). To activate the
163 inflammasome, the cells were treated with 200 ng/mL lipopolysaccharide (LPS) (InvivoGen)
164 at 37°C in 5% CO2 for 4 h followed by treatment with 10 µM nigericin (InvivoGen) for 1 h.
165 For the *in vivo* model, the virus transduction efficiency of the cells was confirmed by flow
166 cytometry at 72 h post-infection. We confirmed the proportion of $RUNX1^{S291fs}CBL^{\Delta E8/9}$ cells,
167 which are positive for both hNGFR (*RUNX1S291fs*) and GFP ($CBL^{\Delta E8/9}$), was greater than
168 10% of c-kit-positive cells. Subsequently, we transplanted bulk c-kit-positive cells containing
169 6×10^6 $CBL^{\Delta E8/9}RUNX1^{S291fs}$ cells via tail vein into congenic recipient mice irradiated with a
170 sublethal dose of 7.0 Gy. PB analysis was performed every 4 weeks after transplantation.
171
172 **_Tet2_-deficient MDS/MPN mouse model**
173 Whole bone marrow (BM) cells (5×10^6) from $Tet2^{fl/fl}$, $Tet2^{fl/fl}$;*Vav1-iCre* and $Tet2^{fl/fl}$;$Asc^{-/-}$;
174 *Vav1-iCre* mice were transplanted via tail vein into congenic recipient mice (Ly5.1) irradiated
175 with lethal doses of radiation (9.5 Gy). PB cells were analyzed every month after
176 transplantation and BM cells were analyzed 5 months later.
177
178 **RNA sequencing and data processing**
179 Total RNA was extracted from 5,000 Lin^{-}c-kit^{+} (LK) cells sorted by FACSAriaIIIu using the
180 RNeasy Plus Micro Kit (Qiagen), and cDNA was synthesized using the SMART-Seq HT Kit
181 (Clontech). Library preparation was performed using the NEBNext Ultra DNA Library Prep
182 Kit for Illumina (New England BioLabs, UK). After checking the concentration of each

183 library on a TapeStation (Agilent), sequencing was performed using NextSeq500 (Illumina)
184 with single-read sequencing. TopHat (version 2.0.13; with default parameters) was used to
185 map reads to the reference genome (UCSC/mm10) using annotation data from iGenomes
186 (Illumina). Gene expression levels were quantified using the Cuffdiff software (version 2.2.1;
187 default parameters).
188
189 **GSEA**
190 Gene set enrichment analysis (GSEA)[22] was performed on the data curated from the Broad
191 Institute's molecular signature database MSigDB. The gene sets used in this study are listed
192 in Table S2**.**
193
194 **Statistical analysis**
195 Statistical analyses were performed using GraphPad Prism version 10. The significance of
196 differences was measured by *one-way* ANOVA, a paired *t*-test, unpaired two-tailed Student's
197 *t*-test, or Welch's *t*-test when variance was judged to be significantly different by the F-test.
198 Data are shown as the mean ± SEM.
199
200 **Accession numbers**
201 The RNA sequencing data were deposited in the DNA Data Bank of Japan (accession number:
202 PRJDB19718).

Results

Inhibitory effect of *Asc* deficiency on inflammasome activation

Because ASC functions not only within the NLRP3 inflammasome but also in various inflammasomes formed by other sensor proteins[5, 6], the loss of ASC is assumed to broadly impact the suppression of inflammasome activation. To elucidate the role of inflammasome activation in MDS progression, we utilized mice deficient in *Asc*[19]. To confirm the inhibitory impact of *Asc*-deficiency on inflammasome activation, we employed peritoneal macrophages, a commonly utilized cellular model in inflammasome research. Ten percent thioglycolate was administered via intraperitoneal injection to wild-type (WT) and *Asc*$^{-/-}$ mice. Lipopolysaccharide (LPS), a component of the cell wall of gram-negative bacteria, and nigericin, an antiporter of hydrogen and potassium ions, induce the activation of NLRP3, a representative sensor protein[23]. Peritoneal macrophages were primed with LPS for 4 hours in a culture medium and then stimulated with nigericin for 1 h to induce inflammasome activation (Supplementary Figure 1A). ASC protein was not detected in *Asc*$^{-/-}$ peritoneal macrophages using western blotting (Supplementary Figure 1B). Priming of peritoneal macrophages by LPS induced increased expression of pro-IL-1β and NLRP3[24], which was observed in both WT and *Asc*$^{-/-}$ peritoneal macrophages, indicating that the priming was normal in *Asc*$^{-/-}$ peritoneal macrophages. Consistent with previous reports, induction of pro-IL-1β was rather enhanced in *Asc*$^{-/-}$ peritoneal macrophages[25]. Activation of inflammasomes by nigericin induces activation of caspase-1, and activated caspase-1 (cleaved caspase-1) converts pro-IL-1β into its activated form. In *Asc*$^{-/-}$ peritoneal macrophages, caspase-1 activation was suppressed, and secretion of activated IL-1β (cleaved IL-1β) into the supernatant was not detected (Supplementary Figure 1B). Upon the formation of the inflammasome complex, ASC adaptor proteins polymerize to form large filament-like clusters called ASC specks[26]. ASC immunostaining showed ASC speck formation in WT

peritoneal macrophages after LPS and Nigericin treatment; however, no speck formation was detected in *Asc*$^{-/-}$ peritoneal macrophages (Supplementary Figure 1C). These results confirmed that *Asc*$^{-/-}$ cells do not form inflammasome complexes and that signals downstream of active inflammasomes are suppressed.

Contribution of inflammasome in steady-state hematopoiesis

To clarify the contribution of inflammasome to steady-state hematopoiesis, we examined PB and bone marrow (BM) in 8-week-old WT and *Asc*$^{-/-}$ mice. Hemoglobin levels and B-cell fraction were slightly increased in the PB of *Asc*$^{-/-}$ mice (Figure 1A). On the other hand, in BM of *Asc*$^{-/-}$ mice, the absolute number of Lin^{-}Sca1^{+}c-kit^{+} (LSK) cells that include HSCs and multipotent progenitor cells, was significantly decreased, while that of HSCs was not affected (Figure 1B).

Next, we examined the repopulation capacity of *Asc*$^{-/-}$ BM cells. BM cells from WT and *Asc*$^{-/-}$ mice (CD45.2) were transplanted into lethally irradiated recipient mice (CD45.1) together with an equal number of competitive BM cells from congenic CD45.1 mice (Figure 1C). *Asc*$^{-/-}$ BM cells established donor chimerism comparable to that of WT BM cells in both PB and BM HSCs at 4 months post-transplantation (Figure 1D). To assess long-term repopulation capacity, BM cells from primary recipient mice were transplanted into lethally irradiated secondary recipient mice (CD45.1). Again, *Asc*$^{-/-}$BM cells established chimerism comparable to that of WT BM cells in PB (Figure 1E), indicating that loss of ASC has little impact on BM repopulation capacity (Figure 1E). In contrast, *Asc*$^{-/-}$ BM cells reproducibly generated a modest but significant increase in the proportion of PB B cells in secondary recipients (Figure 1E). These results indicate that inhibition of inflammasome activation by loss of ASC has a moderate effect on lineage composition of differentiated white blood cells.

ASC loss does not affect the proliferation of *CBL*$^{\Delta E8/9}$*RUNX1*^{S291fs} MDS cells in culture

Analyses of human MDS samples have revealed that activated NLRP3 complexes in HSPCs activate caspase-1, promoting IL-1β and IL-18 production and cell death through pyroptosis[10]. ASC specks were detected in the PB of patients with MDS at a significantly higher frequency than in healthy donors or other hematological malignancies[12]. Further, we evaluated the involvement of the inflammasome pathway in the MDS mouse model. We analyzed the mouse MDS model induced by co-expression of mutant *CBL* (*CBL*$^{\Delta E8/9}$) and *RUNX1* (*RUNX1*^{S291fs})[18]. This MDS model reproduced the phenotypic characteristics of MDS with a short latency[18]. Mechanistically, excessive dynamin-related protein 1 (DRP1)-dependent mitochondrial fragmentation in HSPCs induces excessive production of reactive oxygen species, which activates inflammatory signals, thereby promoting ineffective hematopoiesis.

c-kit$^+$ HSPCs from WT and *Asc*$^{-/-}$ mice were transduced with *CBL*$^{\Delta E8/9}$ and *RUNX1*^{S291fs} retroviruses and subsequently analyzed for cell proliferation *in vitro* (Figure 2A). *CBL*$^{\Delta E8/9}$ and *RUNX1*^{S291fs} cells were marked by GFP and hNGFR expression, respectively. Cells co-expressing *CBL*$^{\Delta E8/9}$ and *RUNX1*^{S291fs} (hereafter referred to as *CBL*$^{\Delta E8/9}$*RUNX1*^{S291fs} cells) were purified by cell sorting (Figure 2B), and equal numbers of sorted cells were cultured for subsequent analyses. At the timing of cell sorting, 3 days after transduction, *CBL*$^{\Delta E8/9}$*RUNX1*^{S291fs} cultures contained an increased proportion of HSPCs, particularly LSK cells. However, none of these phenotypic changes was significantly altered by loss of ASC (Figure 2C). Consistent with these findings, *CBL*$^{\Delta E8/9}$*RUNX1*^{S291fs} cells showed a clear growth advantage over control cells. In addition, *Asc*$^{-/-}$ *CBL*$^{\Delta E8/9}$*RUNX1*^{S291fs} cells exhibited enhanced growth relative to their WT counterparts, although the difference did not reach statistical significance (Figure 2D). On day 15 of culture, control and *CBL*$^{\Delta E8/9}$*RUNX1*^{S291fs} cultures contained approximately the same proportion of differentiated Mac-1$^+$ myeloid cells. Among the myeloid cells, while Ly6G$^+$ neutrophils predominated in control culture, CD115$^+$

monocytes predominated in *CBL*$^{\Delta E8/9}$*RUNX1*^{S291fs} cultures. However, none of these phenotypic changes was significantly altered by loss of ASC (Supplementary Figure 2).

Inflammasome activation can induce pyroptotic cell death through caspase-1–mediated activation of gasdermin D. Pyroptotic cells can exhibit Annexin V and propidium iodide (PI) double positivity; however, this staining pattern alone cannot distinguish pyroptotic cells from late apoptotic cells. On day 8 of culture, cells were challenged with LPS and nigericin to activate the inflammasome, followed by assessment of cell death using Annexin V and PI staining (Figure 2E and F). No significant differences in Annexin V^{+}PI^{-} apoptotic cell death were observed between WT and *Asc*$^{-/-}$ control cells or between WT and *Asc*$^{-/-}$ *CBL*$^{\Delta E8/9}$*RUNX1*^{S291fs} cells. In contrast, *CBL*$^{\Delta E8/9}$*RUNX1*^{S291fs} cells exhibited significantly increased Annexin V^{+}PI^{+} cell death compared with control cells, and this increase was further enhanced by inflammasome activation with LPS and nigericin. Importantly, this effect was significantly attenuated by loss of ASC (Figures 2F and G). We next measured IL-1β levels in the culture supernatants. Although IL-1β levels were below the detection limit under basal conditions, treatment with LPS and nigericin markedly increased IL-1β secretion in both control and *CBL*$^{\Delta E8/9}$*RUNX1*^{S291fs} cells. This induction was completely abolished in *Asc*-deficient cells (Figure 2H). In contrast, IL-18 levels were below the limit of detection (data not shown) and TNFα induction was unaffected by loss of ASC (Figure 2H). Together, these findings indicate that *CBL*$^{\Delta E8/9}$*RUNX1*^{S291fs} cells are more susceptible to inflammasome-dependent pyroptotic cell death and support a role for inflammasome activation in these cells.

ASC loss does not affect the onset and early progression of MDS

We then analyzed the impact of ASC loss in MDS mice. After transduction of c-kit-positive cells from WT and *Asc*$^{-/-}$ mice with *CBL*$^{\Delta E8/9}$ and *RUNX1*^{S291fs} retroviruses, we first confirmed by flow cytometric analysis that the proportion of *CBL*$^{\Delta E8/9}$*RUNX1*^{S291fs} cells was greater than

10% of c-kit-positive cells (Supplementary Figure 3). Subsequently, we transplanted bulk c-kit-positive cells containing 6×10^6 *CBL*$^{\Delta E8/9}$*RUNX1*^{S291fs} cells into congenic recipient mice irradiated with a sublethal dose of 7.0 Gy (WT and *Asc*$^{-/-}$ *CBL*$^{\Delta E8/9}$*RUNX1*^{S291fs} mice, respectively) (Figure 3A).

We then performed a detailed analysis of hematopoiesis in WT and *Asc*$^{-/-}$ *CBL*$^{\Delta E8/9}$*RUNX1*^{S291fs} mice. At 3 months post-transplantation, both WT and *Asc*$^{-/-}$ *CBL*$^{\Delta E8/9}$*RUNX1*^{S291fs} mice developed pancytopenia compared to controls (Figure 3B). The proportion of *CBL*$^{\Delta E8/9}$*RUNX1*^{S291fs} cells was high in myeloid cells but was significantly lower in T cells (Figure 3B). PB smears showed morphological dysplasia such as pseudo-Pelger-Huët nuclear abnormalities and hypersegmented nuclear neutrophils (Figure 3C), as well as giant platelets (data not shown), which are characteristic of MDS. Histological analyses also revealed a significant reduction in the number of mature megakaryocytes in the BM of *CBL*$^{\Delta E8/9}$*RUNX1*^{S291fs} mice (Supplementary Figure 4A and B), indicating impaired megakaryocyte maturation. In contrast, no significant differences were observed between WT and *Asc*$^{-/-}$ *CBL*$^{\Delta E8/9}$*RUNX1*^{S291fs} mice. Furthermore, both WT and *Asc*$^{-/-}$ *RUNX1*^{S291fs}*CBL*$^{\Delta E8/9}$ mice showed increased LK hematopoietic progenitor cells and enhanced cell death of CD45$^+$ hematopoietic cells in BM (Figure 3D and 3G). They also showed a mild block in erythroid differentiation at the transition from stage IV to stage V (Figure 3E and F), along with increased cell death of Ter119$^+$ erythroid cells (Figure 3G), which is consistent with the mild anemia observed in Figure 3B. All these MDS phenotypes were similar between WT and *Asc*$^{-/-}$ *RUNX1*^{S291fs}*CBL*$^{\Delta E8/9}$ mice. Therefore, ASC-mediated inflammasome activation might play a limited role in the onset and early stages of MDS development.

ASC loss prolongs the survival of MDS mice

During a long-term observation of the MDS mice, WT *CBL*$^{\Delta E8/9}$*RUNX1*^{S291fs} mice developed

a lethal disease, and all died 7 months after transplantation (Figure 4A). Notably, *Asc*$^{-/-}$ *CBL*$^{\Delta E8/9}$*RUNX1*^{S291fs} MDS mice showed significantly prolonged survival beyond 10 months after transplantation (Figure 4A). We analyzed moribund mice by flow cytometric analysis of PB and BM and microscopic analysis of PB smears and found that they died of advanced MDS (Figure 4B and Supplementary Figure 5A) or AML (Figure 4C and Supplementary Figure 5B). In AML cases, flow cytometric analysis of PB showed a marked increase in immature cell populations (non-MyBT, leukemic blasts) among CD45^{+} cells that were negative for B- and T-cell differentiation markers and negative or weakly positive for Mac-1, a marker for myeloid cells. PB smears revealed many undifferentiated blast-like cells with an increased nuclear/cytoplasmic ratio (Figure 4C and Supplementary Figure 5B). In the BM of AML mice, hNGFR- and GFP-co-expressing cells, which were mostly c-kit^{+}, were increased. BM cytospin specimens showed an expansion of undifferentiated blast-like cells (data not shown). Therefore, we concluded that the moribund mice converted from MDS to AML. In contrast, moribund mice with lethal MDS did not show a significant increase in immature cell population (non-MyBT) of PB CD45^{+} cells. PB smears showed dysplastic hematopoietic cells but not leukemic blasts (Figure 4B and Supplementary Figure 5A). BM cytospin specimens showed no significant increase in the number of blast-like cells (data not shown). *Asc*$^{-/-}$ *CBL*$^{\Delta E8/9}$*RUNX1*^{S291fs} MDS mice developed AML at similar timing and frequencies to those of WT *CBL*$^{\Delta E8/9}$*RUNX1*^{S291fs} mice (median survival: *Asc*$^{-/-}$ *CBL*$^{\Delta E8/9}$*RUNX1*^{S291fs} AML 176.5 days vs. WT *CBL*$^{\Delta E8/9}$*RUNX1*^{S291fs} AML 162.0 days) (Figure 4A). However, *Asc*$^{-/-}$ *CBL*$^{\Delta E8/9}$*RUNX1*^{S291fs} MDS mice took longer to progress to lethal MDS (median survival: *Asc*$^{-/-}$ *CBL*$^{\Delta E8/9}$*RUNX1*^{S291fs} MDS 262.0 days vs. WT *CBL*$^{\Delta E8/9}$*RUNX1*^{S291fs} MDS 171.0 days), resulting in better overall survival than did WT MDS mice (Figure 4A).

ASC loss attenuates inflammasome activation and MDS progression

PB analysis of MDS mice surviving up to 6 months after transplantation revealed macrocytic anemia with increased mean corpuscular volume (MCV) and thrombocytopenia in both WT and *Asc*$^{-/-}$ MDS mice (Figure 5A). Nonetheless, WT MDS mice showed more progressive macrocytic anemia with markedly increased MCV than did *Asc*$^{-/-}$ MDS mice (Figure 5A). Subsequently, we compared the PB data of WT moribund mice with those of *Asc*$^{-/-}$ mice. Both WT and *Asc*$^{-/-}$ MDS mice that developed AML showed markedly increased white blood cell counts and a significant expansion of non-MyBT immature cell populations in the PB at the moribund stage (Figure 5B, Supplementary Figure 6A). In the case of MDS, while *Asc*$^{-/-}$ mice had extended survival (Figure 4A), they also exhibited advanced pancytopenia comparable to WT MDS mice at the moribund stage (Figure 5B). The proportion of *CBL*$^{\Delta E8/9}$*RUNX1*^{S291fs} cells was high in myeloid cells and non-MyBT cells but significantly lower in B and T cells, regardless of *Asc* status (Supplementary Figure 6B). Collectively, these results indicate loss of ASC slows but does not completely prevent the progression of ineffective hematopoiesis.

To monitor inflammasome activation, we measured IL-1β and IL-18 levels in BM fluid 3 months after transplantation. While IL-1β levels remained very low, IL-18 levels were significantly elevated in *CBL*$^{\Delta E8/9}$*RUNX1*^{S291fs} MDS mice, and this increase was attenuated in the absence of ASC (Figure 5C). We next assessed caspase-1 activation in BM cells at 3 months post-transplantation. The proportion of cells with active caspase-1 was significantly increased in the lineage marker^{-} (Lin^{-}) progenitor fraction, especially in Lin^{-}c-kit^{+}Sca1^{-} myeloid progenitors, from *CBL*$^{\Delta E8/9}$*RUNX1*^{S291fs} MDS mice compared with control mice (Figure 5D). This finding is consistent with a previous report demonstrating active NLRP3 inflammasome complexes in progenitor cells from patients with MDS[10]. Caspase-1 activation was reduced in *Asc*$^{-/-}$ mice, although the difference did not reach statistical significance (Figure 5D). Although the proportion of cells with active caspase-1 in Lin^{+} mature cell fraction was comparable between control and *CBL*$^{\Delta E8/9}$*RUNX1*^{S291fs} MDS mice, caspase-1

activation was higher in Lin^+ cells than in Lin^- cells in both groups and was moderately but significantly reduced in the absence of ASC. These results suggest that inflammasomes are aberrantly activated in myeloid progenitors in the *CBL*$^{\Delta E8/9}$*RUNX1*^{S291fs} MDS model. Given that loss of ASC attenuated MDS progression, reduced inflammasome activity in both myeloid progenitors and differentiated Lin^+ cells may have contributed to the attenuation of disease phenotype.

CBL$^{\Delta E8/9}$RUNX1^{S291fs} MDS cells express inflammatory gene signatures

To understand the effect of ASC loss on inflammasome activation in *CBL*$^{\Delta E8/9}$*RUNX1*^{S291fs} MDS cells, $Lineage^-$c-kit^+ *CBL*$^{\Delta E8/9}$*RUNX1*^{S291fs} MDS progenitor cells from MDS mice 3 months after transplantation were purified by sorting and subjected to RNA sequencing analysis (Supplementary Figure 7A). Principal component analysis (PCA) clearly separated WT control and WT *CBL*$^{\Delta E8/9}$*RUNX1*^{S291fs} cells, whereas *Asc*$^{-/-}$ *CBL*$^{\Delta E8/9}$*RUNX1*^{S291fs} cells were assigned between them (Figure 6A). We identified 793 differentially expressed genes (DEGs) upregulated in WT *CBL*$^{\Delta E8/9}$*RUNX1*^{S291fs} MDS cells compared to WT control cells ($Log_2FC > 1$, P-value < 0.05, Padj < 0.05). Of these, approximately 44% were downregulated by loss of ASC in MDS cells (Figure 6B, Supplementary Figure 7B, and Supplementary Table 1). Gene set enrichment analysis (GSEA) revealed that various inflammatory signaling genes (inflammasome, IL1 and IL18 signaling, interferon response, and apoptosis) tended to be upregulated in WT *CBL*$^{\Delta E8/9}$*RUNX1*^{S291fs} MDS cells compared to WT control cells, and their expression was downregulated in the absence of ASC (Figure 6C, 6D and Supplementary Table 2). A heatmap of inflammation- and MDS-related DEGs in WT *CBL*$^{\Delta E8/9}$*RUNX1*^{S291fs} MDS cells demonstrated that the majority of these transcriptional changes were attenuated in *Asc*$^{-/-}$ *CBL*$^{\Delta E8/9}$*RUNX1*^{S291fs} MDS cells (Figure 6D and 6E). Collectively, these results support a role for ASC in regulating inflammatory responses and suggest that loss of ASC alleviates

inflammatory signaling in MDS. Expression of gene sets involved in cell proliferation, ribosomal biogenesis, and protein synthesis, which were downregulated in WT *CBL*$^{\Delta E8/9}$*RUNX1*^{S291fs} MDS cells, was restored in *Asc*$^{-/-}$ *CBL*$^{\Delta E8/9}$*RUNX1*^{S291fs} MDS cells. Furthermore, a gene set associated with MDS risk was moderately downregulated in *Asc*$^{-/-}$ *CBL*$^{\Delta E8/9}$*RUNX1*^{S291fs} MDS cells (Figure 6D and 6E). These findings are consistent with the perturbed MDS progression in *Asc*$^{-/-}$ MDS mice.

ASC loss attenuates *Tet2* deficiency-mediated MDS/MPN progression

To assess whether the role of ASC extends to additional MDS models, we next examined a *Tet2*-deficient model. BM cells from *Tet2*$^{fl/fl}$;*Vav1-iCre* mice were transplanted into lethally irradiated recipient mice, and disease progression was evaluated in the presence and absence of ASC (Figure 7A). Consistent with previous reports[27], *Tet2*-deficient BM cells developed MDS-like disease, and a subset of mice died during the observation period (Figure 7B). These mice exhibited pancytopenia (Figure 7C), mild myeloid-biased differentiation (Figure 7D), expansion of BM HSPCs (Figure 7E), and a mild block in erythroid differentiation at the transition from stage IV to stage V (Figure 7F), accompanied by increased cell death of Ter119^{+} erythroid cells (Figure 7G). These phenotypes were largely consistent with those observed in the *CBL*$^{\Delta E8/9}$*RUNX1*^{S291fs} MDS model. Notably, *Asc* deficiency substantially attenuated the MDS phenotypes induced by *Tet2* deficiency. In this model, IL-1β and IL-18 levels were markedly elevated in BM fluid, and these increases were reduced in the absence of ASC, particularly in the case of IL-1β (Figure 7H). These findings provide additional evidence supporting the requirement for ASC-dependent inflammasome activation in MDS progression.

Discussion

In this study, we attempted to clarify the pathogenic significance of the inflammasome in MDS using mice lacking ASC, an adaptor protein that forms the inflammasome. Under steady-state conditions, the loss of ASC did not impair the function of HSPCs. Because inflammasome activation is suppressed at a low level under steady-state conditions, inflammasome inactivation is not thought to cause a significant impairment of normal hematopoiesis. Conversely, in the MDS mouse models, the loss of ASC significantly extended survival time.

In the *CBL*$^{\Delta E8/9}$*RUNX1*^{S291fs} MDS mouse model, no significant differences were observed in the initiation of MDS between WT and *Asc*$^{-/-}$ cells. On the other hand, *Asc*$^{-/-}$ *CBL*$^{\Delta E8/9}$*RUNX1*^{S291fs} mice showed significantly attenuated progression of cytopenia and development of lethal MDS, resulting in significantly longer survival than WT *CBL*$^{\Delta E8/9}$*RUNX1*^{S291fs} mice. Notably, *Asc* deficiency also substantially attenuated the MDS phenotypes induced by *Tet2* deficiency. These results are consistent with those from a previous observation that the inhibition of NLRP3 or caspase-1 improves the ineffective hematopoiesis of human MDS samples in culture[10]. Collectively, these findings support a role for inflammasome activation in exacerbating ineffective hematopoiesis and promoting MDS progression.

Various stimuli induce inflammasome activation in MDS cells. DAMPs derived from damaged cells, such as S100A8/9, are well-known inducers of inflammasome signaling[28], and their levels may increase with MDS progression. However, this study did not longitudinally assess inflammasome activation levels across different disease stages, from MDS onset through advanced disease, and leukemic transformation. Defining the kinetics of inflammasome activation during disease progression will therefore be an important subject for future studies. In addition, the roles of IL-1β and IL-18, key inflammatory cytokines

451 produced downstream of inflammasome signaling pathways, in MDS progression and
452 particularly in ineffective hematopoiesis warrant further investigation. In WT
453 *CBL*$^{\Delta E8/9}$*RUNX1*^{S291fs} MDS mice, IL-1β levels remained very low, although IL-1β production
454 could be induced in cultured cells by LPS and nigericin treatment. In contrast, IL-18 levels
455 were significantly elevated in *Asc*-dependent manner. In *Tet2*-deficient MDS mice, both IL-
456 1β and IL-18 levels were elevated, and these increases were attenuated by *Asc* deficiency,
457 particularly for IL-1β. Pro-IL-18 is constitutively expressed in many cell types, whereas IL-
458 1β production generally requires transcriptional induction of pro- IL-1β by inflammatory
459 stimuli before inflammasome-dependent processing[29]. Thus, the differential patterns of IL-1β
460 and IL-18 production may reflect more robust inflammatory priming in *Tet2*-deficient MDS
461 than in *CBL*$^{\Delta E8/9}$*RUNX1*^{S291fs} MDS and suggest that the mechanisms regulating
462 inflammasome responses differ between these two disease models.

463 Clonal hematopoiesis of indeterminate potential (CHIP), characterized by the age-
464 associated expansion of HSC clones harboring acquired somatic mutations, is closely
465 associated with the development of MDS[30, 31]. Inflammation and immune dysregulation can
466 promote clonal hematopoiesis[32], raising an important question of whether inflammasome
467 activity contributes to the establishment or expansion of CHIP. The NLRP3 inflammasome
468 has also been implicated in the progression of myeloproliferative neoplasms and *de novo*
469 AML, in part through IL-1β-mediated mechanisms[33,34]. In the present study, however,
470 *CBL*$^{\Delta E8/9}$*RUNX1*^{S291fs} MDS progressed to AML with similar timing and frequency regardless
471 of *Asc* status, despite the attenuation of MDS progression and prolonged survival associated
472 with *Asc* deficiency. These findings suggest that ASC-dependent inflammasome signaling
473 contributes to MDS progression but may have a limited role in leukemic transformation in
474 this model. Thus, the biological consequences of inflammasome activation may differ
475 according to the genetic context, type of myeloid malignancy, and disease stage[9]. Although

findings from the *CBL*$^{\Delta E8/9}$*RUNX1*^{S291fs} MDS model cannot be generalized to all forms of MDS, further investigation of the roles of inflammasome signaling during clonal hematopoiesis, MDS progression, and secondary AML development may provide a more comprehensive understanding of MDS pathogenesis.

Transcriptome analysis revealed increased expression of inflammatory response-associated genes and decreased expression of genes involved in cell proliferation and protein synthesis in *CBL*$^{\Delta E8/9}$*RUNX1*^{S291fs} MDS cells. These transcriptional alterations were partially reversed by *Asc* deficiency, consistent with the attenuation of cytopenia observed in *Asc*$^{-/-}$ MDS mice compared with WT MDS mice. IL-18 produced downstream of inflammasome activation is known to induce interferon γ[35], which in turn can upregulate the expression of inflammasome components, including *ASC*, *NLRC4*, and *NLRP3*[36]. Therefore, inflammasome activation and interferon γ signaling may form a positive feedback loop that amplifies inflammatory responses in MDS. *Asc* deficiency may disrupt this crosstalk, thereby attenuating inflammation and limiting disease progression.

Finally, because ASC is involved in the formation of numerous inflammasomes[5, 6], it is currently unclear which sensor proteins are involved in inflammasomes in the *CBL*$^{\Delta E8/9}$*RUNX1*^{S291fs} and *Tet2*-deficient MDS models. Although the involvement of NLRP3 in MDS has already been reported[10], there are diverse abnormalities related to innate immunity in MDS. Thus, various inflammasomes may be activated. Recently, it was reported that Bruton's tyrosine kinase (BTK) is essential for NLRP3 inflammasome formation and that ibrutinib, a BTK inhibitor, inhibits NLRP3 inflammasome formation[37]. Several compounds that inhibit ASC polymerization have also been reported[38-40], which may have clinical applications in the future. Understanding the types of inflammasomes involved in MDS and their ligands is important for understanding the pathogenesis of MDS.

Acknowledgments

We would like to thank Hideki Hara for the valuable discussions and Ola Rizq for a critical review of our manuscript. Supercomputing resources were provided by the Human Genome Center at the Institute of Medical Science, University of Tokyo, Japan. This work was supported in part by Grants-in-Aid for Scientific Research (19H05653, 19H05746, 24H00066 to AI, and 23K07806 to Y.N-T) from the Japan Society for the Promotion of Science (JSPS), Moonshot (21zf0127003h0001 to AI), ASPIRE (25jf0126013h0001), and UTOPIA (JP243fa627001 to AI) projects from AMED, Japan, the Takeda Science Foundation (to Y.N-T) and the Naito Science & Engineering Foundation (to Y.N-T).

Author contributions

S.A. and Y.N-T. performed the experiments, analyzed the results, created the figures, and actively wrote the manuscript; Y.N-T secured funding; S.U., Y.A., T.F., M.M., A.T., S.K., M.O., and T.N. assisted with the experiments; B.R. and A.K. performed sequencing; S.T. provided the mice; Y.N. discussed the results; Y.H. and H.H. provided materials and discussed the results; A.I. conceived and directed the project, secured funding, and wrote the manuscript actively.

Disclosure of Conflicts of Interest

The authors have no competing interests to declare.

References

1. Sekeres MA, Taylor J. Diagnosis and Treatment of Myelodysplastic Syndromes: A Review. *JAMA* 2022 Sep 6; **328**(9)**:** 872-880.

2. Greenberg P, Cox C, LeBeau MM, Fenaux P, Morel P, Sanz G*, et al.* International scoring system for evaluating prognosis in myelodysplastic syndromes. *Blood* 1997 Mar 15; **89**(6)**:** 2079-2088.

3. Fenaux P, Mufti GJ, Hellstrom-Lindberg E, Santini V, Finelli C, Giagounidis A*, et al.* Efficacy of azacitidine compared with that of conventional care regimens in the treatment of higher-risk myelodysplastic syndromes: a randomised, open-label, phase III study. *Lancet Oncol* 2009 Mar; **10**(3)**:** 223-232.

4. Fenaux P, Giagounidis A, Selleslag D, Beyne-Rauzy O, Mufti G, Mittelman M*, et al.* A randomized phase 3 study of lenalidomide versus placebo in RBC transfusion-dependent patients with Low-/Intermediate-1-risk myelodysplastic syndromes with del5q. *Blood* 2011 Oct 6; **118**(14)**:** 3765-3776.

5. Xue Y, Enosi Tuipulotu D, Tan WH, Kay C, Man SM. Emerging Activators and Regulators of Inflammasomes and Pyroptosis. *Trends Immunol* 2019 Nov; **40**(11)**:** 1035-1052.

6. Karki R, Kanneganti TD. Diverging inflammasome signals in tumorigenesis and potential targeting. *Nat Rev Cancer* 2019 Apr; **19**(4)**:** 197-214.

7. Devant P, Kagan JC. Molecular mechanisms of gasdermin D pore-forming activity. *Nat Immunol* 2023 Jul; **24**(7)**:** 1064-1075.

8. Sallman DA, List A. The central role of inflammatory signaling in the pathogenesis of myelodysplastic syndromes. *Blood* 2019 Mar 7; **133**(10)**:** 1039-1048.

9. Andina N, Bonadies N, Allam R. Inflammasome Activation in Myeloid Malignancies-Friend or Foe? *Front Cell Dev Biol* 2021; **9:** 825611.

10. Basiorka AA, McGraw KL, Eksioglu EA, Chen X, Johnson J, Zhang L*, et al.* The NLRP3 inflammasome functions as a driver of the myelodysplastic syndrome phenotype. *Blood* 2016 Dec 22; **128**(25)**:** 2960-2975.

11. Sallman DA, Cluzeau T, Basiorka AA, List A. Unraveling the Pathogenesis of MDS: The NLRP3 Inflammasome and Pyroptosis Drive the MDS Phenotype. *Front Oncol* 2016; **6:** 151.

12. Basiorka AA, McGraw KL, Abbas-Aghababazadeh F, McLemore AF, Vincelette ND, Ward GA*, et al.* Assessment of ASC specks as a putative biomarker of pyroptosis in myelodysplastic syndromes: an observational cohort study. *Lancet Haematol* 2018 Sep; **5**(9)**:** e393-e402.

13. Harada H, Harada Y, Niimi H, Kyo T, Kimura A, Inaba T. High incidence of somatic mutations in the AML1/RUNX1 gene in myelodysplastic syndrome and low blast

percentage myeloid leukemia with myelodysplasia. *Blood* 2004 Mar 15; **103**(6)**:** 2316-2324.

14. Makishima H, Cazzolli H, Szpurka H, Dunbar A, Tiu R, Huh J*, et al.* Mutations of e3 ubiquitin ligase cbl family members constitute a novel common pathogenic lesion in myeloid malignancies. *J Clin Oncol* 2009 Dec 20; **27**(36)**:** 6109-6116.

15. Ogawa S. Genetics of MDS. *Blood* 2019 Mar 7; **133**(10)**:** 1049-1059.

16. Watanabe-Okochi N, Kitaura J, Ono R, Harada H, Harada Y, Komeno Y*, et al.* AML1 mutations induced MDS and MDS/AML in a mouse BMT model. *Blood* 2008 Apr 15; **111**(8)**:** 4297-4308.

17. Nakata Y, Ueda T, Nagamachi A, Yamasaki N, Ikeda KI, Sera Y*, et al.* Acquired expression of Cbl(Q367P) in mice induces dysplastic myelopoiesis mimicking chronic myelomonocytic leukemia. *Blood* 2017 Apr 13; **129**(15)**:** 2148-2160.

18. Aoyagi Y, Hayashi Y, Harada Y, Choi K, Matsunuma N, Sadato D*, et al.* Mitochondrial Fragmentation Triggers Ineffective Hematopoiesis in Myelodysplastic Syndromes. *Cancer Discov* 2022 Jan; **12**(1)**:** 250-269.

19. Yamamoto M, Yaginuma K, Tsutsui H, Sagara J, Guan X, Seki E*, et al.* ASC is essential for LPS-induced activation of procaspase-1 independently of TLR-associated signal adaptor molecules. *Genes Cells* 2004 Nov; **9**(11)**:** 1055-1067.

20. de Boer J, Williams A, Skavdis G, Harker N, Coles M, Tolaini M*, et al.* Transgenic mice with hematopoietic and lymphoid specific expression of Cre. *Eur J Immunol* 2003 Feb; **33**(2)**:** 314-325.

21. Moran-Crusio K, Reavie L, Shih A, Abdel-Wahab O, Ndiaye-Lobry D, Lobry C*, et al.* Tet2 loss leads to increased hematopoietic stem cell self-renewal and myeloid transformation. *Cancer Cell* 2011 Jul 12; **20**(1)**:** 11-24.

22. Subramanian A, Tamayo P, Mootha VK, Mukherjee S, Ebert BL, Gillette MA*, et al.* Gene set enrichment analysis: a knowledge-based approach for interpreting genome-wide expression profiles. *Proc Natl Acad Sci U S A* 2005 Oct 25; **102**(43)**:** 15545-15550.

23. Mariathasan S, Weiss DS, Newton K, McBride J, O'Rourke K, Roose-Girma M*, et al.* Cryopyrin activates the inflammasome in response to toxins and ATP. *Nature* 2006 Mar 9; **440**(7081)**:** 228-232.

24. Bauernfeind FG, Horvath G, Stutz A, Alnemri ES, MacDonald K, Speert D*, et al.* Cutting edge: NF-kappaB activating pattern recognition and cytokine receptors license NLRP3 inflammasome activation by regulating NLRP3 expression. *J Immunol* 2009 Jul 15; **183**(2)**:** 787-791.

25. Conos SA, Lawlor KE, Vaux DL, Vince JE, Lindqvist LM. Cell death is not essential for caspase-1-mediated interleukin-1beta activation and secretion. *Cell Death Differ* 2016 Nov 1; **23**(11)**:** 1827-1838.

26. Martinon F, Burns K, Tschopp J. The inflammasome: a molecular platform triggering activation of inflammatory caspases and processing of proIL-beta. *Mol Cell* 2002 Aug; **10**(2)**:** 417-426.

27. Yokomizo-Nakano T, Hamashima A, Kubota S, Bai J, Sorin S, Sun Y*, et al.* Exposure to microbial products followed by loss of Tet2 promotes myelodysplastic syndrome via remodeling HSCs. *J Exp Med* 2023 Jul 3; **220**(7).

28. Simard JC, Cesaro A, Chapeton-Montes J, Tardif M, Antoine F, Girard D*, et al.* S100A8 and S100A9 induce cytokine expression and regulate the NLRP3 inflammasome via ROS-dependent activation of NF-kappaB(1.). *PLoS One* 2013; **8**(8)**:** e72138.

29. Zhu Q, Kanneganti TD. Cutting Edge: Distinct Regulatory Mechanisms Control Proinflammatory Cytokines IL-18 and IL-1beta. *J Immunol* 2017 Jun 1; **198**(11)**:** 4210-4215.

30. Genovese G, Kahler AK, Handsaker RE, Lindberg J, Rose SA, Bakhoum SF*, et al.* Clonal hematopoiesis and blood-cancer risk inferred from blood DNA sequence. *N Engl J Med* 2014 Dec 25; **371**(26)**:** 2477-2487.

31. Jaiswal S, Fontanillas P, Flannick J, Manning A, Grauman PV, Mar BG*, et al.* Age-related clonal hematopoiesis associated with adverse outcomes. *N Engl J Med* 2014 Dec 25; **371**(26)**:** 2488-2498.

32. Belizaire R, Wong WJ, Robinette ML, Ebert BL. Clonal haematopoiesis and dysregulation of the immune system. *Nat Rev Immunol* 2023 Sep; **23**(9)**:** 595-610.

33. Zhong C, Wang R, Hua M, Zhang C, Han F, Xu M*, et al.* NLRP3 Inflammasome Promotes the Progression of Acute Myeloid Leukemia via IL-1beta Pathway. *Front Immunol* 2021; **12:** 661939.

34. Hamarsheh S, Osswald L, Saller BS, Unger S, De Feo D, Vinnakota JM*, et al.* Oncogenic Kras(G12D) causes myeloproliferation via NLRP3 inflammasome activation. *Nat Commun* 2020 Apr 3; **11**(1)**:** 1659.

35. Nakanishi K. Unique Action of Interleukin-18 on T Cells and Other Immune Cells. *Front Immunol* 2018; **9:** 763.

36. Pilla DM, Hagar JA, Haldar AK, Mason AK, Degrandi D, Pfeffer K*, et al.* Guanylate binding proteins promote caspase-11-dependent pyroptosis in response to cytoplasmic LPS. *Proc Natl Acad Sci U S A* 2014 Apr 22; **111**(16)**:** 6046-6051.

37. Ito M, Shichita T, Okada M, Komine R, Noguchi Y, Yoshimura A*, et al.* Bruton's tyrosine kinase is essential for NLRP3 inflammasome activation and contributes to ischaemic brain injury. *Nat Commun* 2015 Jun 10; **6:** 7360.

38. Soriano-Teruel PM, Garcia-Lainez G, Marco-Salvador M, Pardo J, Arias M, DeFord C*, et al.* Identification of an ASC oligomerization inhibitor for the treatment of

inflammatory diseases. *Cell Death Dis* 2021 Dec 13; **12**(12)**:** 1155.

39. Liu W, Yang J, Fang S, Jiao C, Gao J, Zhang A*, et al.* Spirodalesol analog 8A inhibits NLRP3 inflammasome activation and attenuates inflammatory disease by directly targeting adaptor protein ASC. *J Biol Chem* 2022 Dec; **298**(12)**:** 102696.

40. Chen C, Zhou Y, Ning X, Li S, Xue D, Wei C*, et al.* Directly targeting ASC by lonidamine alleviates inflammasome-driven diseases. *J Neuroinflammation* 2022 Dec 28; **19**(1)**:** 315.

Figure legends

Figure 1. *Asc*$^{-/-}$ mice show normal hematopoiesis

(A) Peripheral blood white blood cell (WBC) counts, hemoglobin (Hb) levels, platelet (Plt) counts, and lineage distribution of differentiated white blood cells (myeloid cells, B cells, and T cells) in 8-week-old WT and *Asc*$^{-/-}$ mice. (B) Numbers of BM cells, HSCs, LSK stem and progenitor cells, and myeloid progenitors (CMP, GMP, and MEP) in 8-week-old WT and *Asc*$^{-/-}$ mice. (C) Experimental design of serial competitive transplantation assays. BM cells (5×10^6 cells) from 8-week-old CD45.2 wild-type and *Asc*$^{-/-}$ mice were transplanted together with the same number of competitor BM cells from CD45.1 congenic mice into recipient mice after lethal irradiation of 9.5 Gy (primary transplantation). Four months later, BM cells (5×10^6 cells) from the primary recipient mice were transplanted into secondary recipient mice after lethal irradiation of 9.5 Gy (secondary transplantation). (D) Percentage of CD45.2 donor-derived cells among PB CD45-positive nucleated cells (CD45.1+CD45.2) in primary recipient mice (upper left panel). Donor chimerism within myeloid cells, B cells, and T cells (lower left panel), and donor-derived HSC chimerism in BM (lower right panel) at 4 months post-transplantation. The lineage composition of PB differentiated white blood cells (myeloid cells, B cells, and T cells) is shown in the upper right panel. (E) Percentage of CD45.2 donor-derived cells among PB CD45-positive nucleated blood cells (CD45.1+CD45.2) in secondary recipient mice (upper panel). The lineage composition of PB differentiated white blood cells (myeloid cells, B cells, and T cells) at 3 months post-transplantation is shown in the lower panel. Significant differences between the two groups by *t*-test are indicated with an asterisk. *p <0.05, **p < 0.01, ***p < 0.001, n.s., not significant.

Figure 2. *CBL*$^{\Delta E8/9}$*RUNX1*^{S291fs} cells are more susceptible to inflammasome-dependent

706 **pyroptotic cell death**

707 (A) Experimental design. c-kit positive HSPCs were purified from wild-type and *Asc*$^{-/-}$ mice
708 and transduced with retroviruses expressing *CBL*$^{\Delta E8/9}$ and *RUNX1S291fs*, which harbor *GFP*
709 and human *NGFR* marker genes, respectively. Co-transduced cells were purified by flow
710 cytometric sorting and cultured in medium containing SCF (50 ng/mL), TPO (50 ng/mL), IL-
711 3 (20 ng/mL), and GM-CSF (20 ng/mL). (B) Representative flow cytometry plots of
712 transduced cells. GFP (*CBL*$^{\Delta E8/9}$) and hNGFR (*RUNX1S291fs*) double-positive (DP) cells
713 were sorted 3 days after virus transduction. (C) Proportion of HSPCs, GMPs and cKit^{-} cells
714 in Lin^{-} GFP and hNGFR double-positive cells 3 days after virus transduction. Significant
715 differences between the two groups by *one-way* ANOVA are indicated with an asterisk.
716 (D)Growth curves of wild-type and *Asc*$^{-/-}$ *CBL*$^{\Delta E8/9}$*RUNX1*^{S291fs} cells. Significant differences
717 on day 21 of culture between the two groups by *t*-test are indicated with an asterisk. (E-G)
718 Experimental design of cell death analyses (E). Cultured cells were treated with LPS and
719 Nigericin on day 8 of culture and subsequently stained with Annexin V and PI. Representative
720 flow cytometry plots (F) and the quantification of Annexin V^{+}PI^{-} and Annexin V^{+}PI^{+} dead
721 cells (G) are shown. (H) IL-1β and TNFα levels in the culture supernatants on day 8 of culture.
722 Significant differences between the two groups by *t*-test are indicated with an asterisk. *p
723 <0.05, **p<0.01, ***p<0.001, ****p <0.0001, n.s., not significant, N.D., not detected.
724
725 **Figure 3. ASC loss does not affect the onset and early progression of MDS**
726 (A) Experimental design for generating MDS mouse models. c-kit positive cells from wild-
727 type and *Asc*$^{-/-}$ mice were transduced with *CBL*$^{\Delta E8/9}$ and *RUNX1*^{S291fs} retroviruses, and the
728 proportion of cells co-expressing *CBL*$^{\Delta E8/9}$ and *RUNX1S291fs* (*CBL*$^{\Delta E8/9}$*RUNX1*^{S291fs} cells)
729 was confirmed to be greater than 10% by flow cytometry analysis. Subsequently, whole
730 cultured cells containing 6 × 10^{6} *CBL*$^{\Delta E8/9}$*RUNX1*^{S291fs} cells were transplanted into congenic

recipient mice irradiated with a sublethal dose of 7.0 Gy. (B) WBC counts, Hb values, mean corpuscular volumes (MCV), and Plt counts (upper). Absolute numbers of myeloid cells, B cells, and T cells, as well as the proportions of GFP (*CBL*$^{\Delta E8/9}$) and hNGFR (*RUNX1S291fs*) double-positive (DP) *CBL*$^{\Delta E8/9}$*RUNX1*^{S291fs} cells within myeloid, B, and T cell populations in PB, are also shown (lower). (C) Images of PB smears observed by May-Grünwald-Giemsa staining. Pseudo-Pelger-Huët nuclear anomaly (left panels) and hypersegmented neutrophils (right panels). (D) Bone marrow cell counts (a pair of femur and tibia), chimerism of CD45.2 donor-derived cells in BM CD45$^+$ nucleated blood cells (CD45.1+CD45.2), numbers of LK progenitor cells in BM. The proportions of *CBL*$^{\Delta E8/9}$*RUNX1*^{S291fs} (DP) cells within total BM and LK cells are also shown. (E) Analysis of erythroid cells in BM. Representative flow cytometry plots of PI-negative cells are shown. Gates defining the erythroid differentiation stages (I-VI) are indicated. (F) Frequencies of cells in each erythroid differentiation stage in Ter119$^+$ erythroid cell. The proportions of *CBL*$^{\Delta E8/9}$*RUNX1*^{S291fs} (DP) cells within each erythroid differentiation stage, are also shown. Asterisks indicate a significant difference compared to stage I. (G) Percentages of Annexin V$^+$PI$^+$ dead cells among CD45$^+$ blood cells and Ter119$^+$ erythroid cells. Statistical analyses were performed by *one-way* ANOVA, and significant differences between the groups are indicated with asterisks. *p <0.05, **p<0.01, n.s., not significant.

Figure 4. ASC loss prolongs survival of *CBL*$^{\Delta E8/9}$*RUNX1*^{S291fs} MDS mice

(A) Survival curve of recipient mice (left panel). In the WT group, four mice died of MDS (green circles), and another four died of AML (black circles). In the *Asc*-deficient group, four mice died of MDS and six mice died of AML. Median survivals are shown in the right panel. Significant differences between the two groups based on the log rank test is indicated with asterisks. **p<0.01. (B, C) A representative WT *CBL*$^{\Delta E8/9}$*RUNX1*^{S291fs} MDS mice that died of

advanced MDS (B) and AML (C). Flow cytometry plots of PB and BM (left and right, respectively). Images of PB smears (center).

Figure 5. Loss of ASC reduces inflammasome activation, thereby attenuating MDS progression

(A) PB cell count data up to 6 months after transplantation. WBC counts, Hb values, MCV, and Plt counts are indicated. Statistical analysis was performed using *one-way* ANOVA. Red and blue asterisks indicate a significant difference of $p < 0.05$ in the comparison of WT *CBL*$^{\Delta E8/9}$*RUNX1*^{S291fs} MDS vs. WT control mice and *Asc*$^{-/-}$ *CBL*$^{\Delta E8/9}$*RUNX1*^{S291fs} MDS vs. *Asc*$^{-/-}$ control mice, respectively. (B) PB counts for MDS and AML mice at their moribund stages and control mice at 7 months post-transplantation. Statistical analysis was performed using the *t*-test. * $p<0.05$, n.s., not significant. (C) IL-1β and IL-18 levels in BM fluids 3 months post-transplantation. Statistical analyses were performed by *one-way* ANOVA are indicated with asterisks. (D) Analysis of Caspase-1 activation by flow cytometry. Activated caspase-1 was detected by reaction with a fluorescent probe-labeled caspase inhibitor in *CBL*$^{\Delta E8/9}$*RUNX1*^{S291fs} mice at 12 weeks post-transplantation. Representative flow cytometry histograms of Lin$^+$ cells and Lin$^-$c-kit$^+$Sca1$^-$ myeloid progenitors (left panels) and percentages of cells with active Caspase-1 in Lin$^+$ cells, Lin$^-$ cells, Lin$^-$c-kit$^+$Sca1$^-$ myeloid progenitors, and LSK cells in bar graphs (right panels) are shown. Significant differences between two groups based on the *t*-test are indicated. * $p<0.05$, ** $p<0.01$, *** $p<0.001$.

Figure 6. Attenuated inflammation-related gene signature in *Asc*$^{-/-}$ MDS mice progenitors

(A) Principal component analysis (PCA) plot based on gene expression by RNA sequencing of Lin$^-$c-kit$^+$ progenitors co-expressing *CBL*$^{\Delta E8/9}$ and *RUNX1*^{S291fs} from MDS mice 3 months

after transplantation. Lin$^-$c-kit$^+$ progenitors were sorted from GFP$^+$hNGFR$^+$ double positive (DP) cells. For the control groups, because of the low frequency of DP cells, Lin$^-$c-kit$^+$ progenitors were sorted from GFP$^+$ and/or hNGFR$^+$ cells. (B) A Venn diagram showing the overlap between up-regulated DEGs in WT *CBL*$^{\Delta E8/9}$*RUNX1*^{S291fs} compared to WT control and down-regulated DEGs in *Asc*$^{-/-}$ *CBL*$^{\Delta E8/9}$*RUNX1*^{S291fs} compared to WT *CBL*$^{\Delta E8/9}$*RUNX1*^{S291fs}. (C) Representative GSEA plots. The normalized enrichment score (NES) values, NOM p-values (p-val), and FDR q-values (q-val) are shown in the plots. (D) Summary of GSEA. (E) Heatmap of the expression of DEGs included in the inflammation- and MDS-related gene sets shown in (D).

Figure 7. ASC loss attenuates *Tet2* deficiency-mediated MDS/MPN progression

(A) Experimental design. BM cells (5 × 10^6 cells) from *Tet2*$^{fl/fl}$*;Vav1-iCre* mice were transplanted into lethally irradiated recipient mice, and disease progression was evaluated in the presence and absence of ASC. (B) Survival curves of recipient mice. PB and BM analyses, as well as ELISA measurements of cytokines, were performed at 5 months post-transplantation. (C) PB WBC counts, Hb levels, MCV, Plt counts, and absolute numbers of myeloid cells, B cells, and T cells. (D) Lineage distribution of differentiated white blood cells (myeloid cells, B cells, and T cells) shown in (C). Significant differences compared with *Tet2*$^{fl/fl}$ by *t*-test are indicated with an asterisk. (E) Chimerism of donor-derived cells in BM and absolute numbers of BM cells, LSK HSPCs, and GMPs. (F) Frequencies of cells in each erythroid differentiation stage. (G) Percentages of Annexin V$^+$PI$^+$ dead cells among CD45.2$^+$ donor-derived cells and Ter119$^+$ erythroid cells. (H) IL-1β and IL-18 levels in BM fluids. Statistical analysis in (C), (E), (F), (G), and (H) were performed by *one-way* ANOVA, and significant differences between the groups are indicated with asterisks. *p <0.05, **p<0.01, ***p<0.001, ****p <0.0001, n.s., not significant.

Figure 1

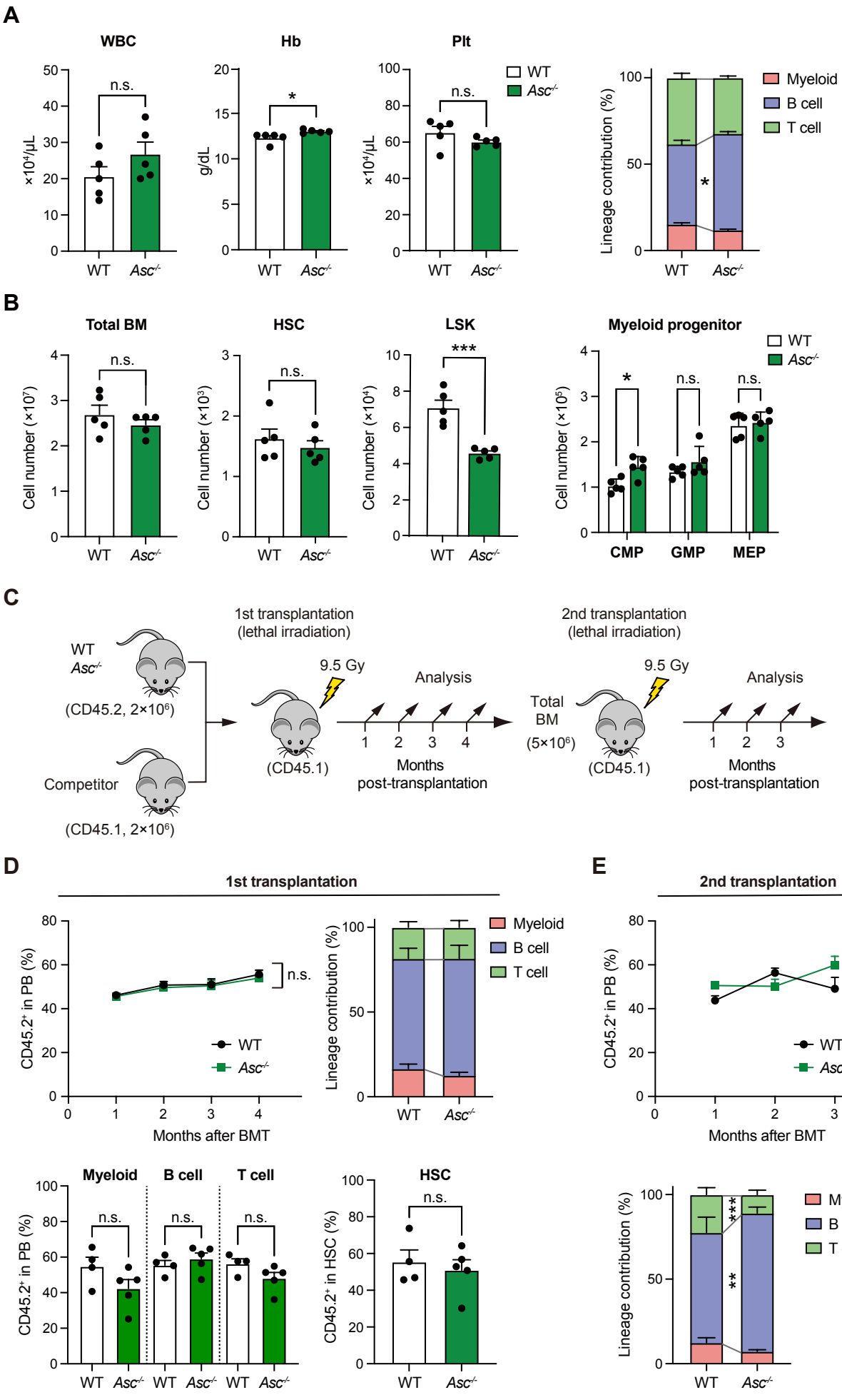

A
WBC
Hb
Plt
n.s.
*
n.s.
WT
Asc-/-
×10⁴/μL
g/dL
Lineage contribution (%)
Myeloid
B cell
T cell
B
Total BM
HSC
LSK
Myeloid progenitor
***
CMP
GMP
MEP
Cell number (×10⁷)
Cell number (×10³)
Cell number (×10⁴)
Cell number (×10⁵)
C
1st transplantation
(lethal irradiation)
2nd transplantation
(lethal irradiation)
9.5 Gy
Analysis
WT
Asc-/-
(CD45.2, 2×10⁶)
Competitor
(CD45.1, 2×10⁶)
(CD45.1)
Total BM
(5×10⁶)
Months post-transplantation
D
1st transplantation
CD45.2⁺ in PB (%)
Months after BMT
Lineage contribution (%)
Myeloid
B cell
T cell
HSC
CD45.2⁺ in HSC (%)
E
2nd transplantation
**

Figure 2

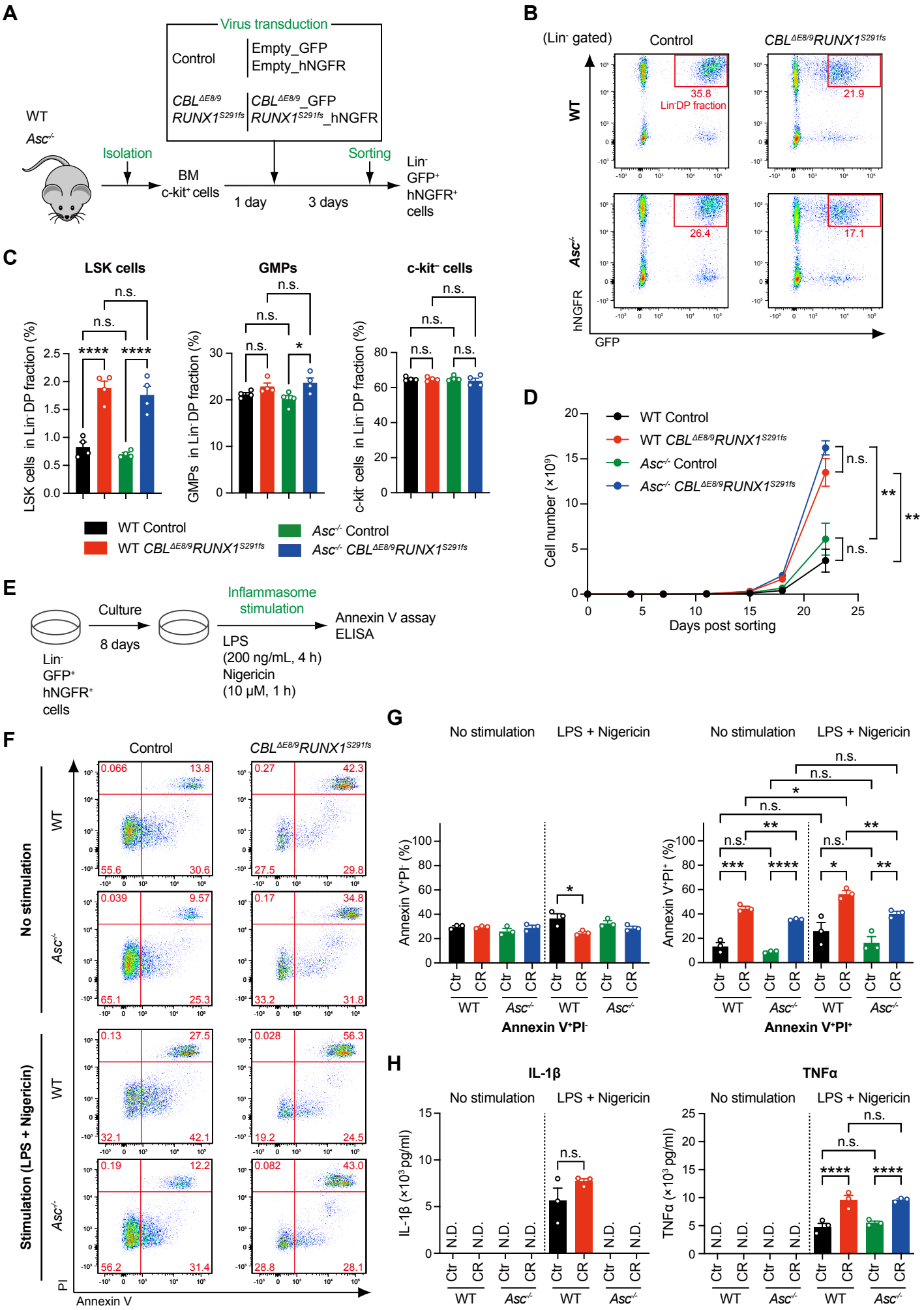

A
Virus transduction
Control
Empty_GFP
Empty_hNGFR
CBL^ΔE8/9 RUNX1^S291fs
CBL^ΔE8/9_GFP
RUNX1^S291fs_hNGFR
WT
Asc-/-
Isolation
BM
c-kit+ cells
1 day
Sorting
3 days
Lin- GFP+ hNGFR+ cells
B
(Lin- gated)
Control
CBL^ΔE8/9RUNX1^S291fs
WT
Asc-/-
35.8
Lin- DP fraction
21.9
26.4
17.1
hNGFR
GFP
C
LSK cells
GMPs
c-kit- cells
LSK cells in Lin- DP fraction (%)
GMPs in Lin- DP fraction (%)
c-kit- cells in Lin- DP fraction (%)
n.s.
****
*
WT Control
WT CBL^ΔE8/9RUNX1^S291fs
Asc-/- Control
Asc-/- CBL^ΔE8/9RUNX1^S291fs
D
Cell number (×10^6)
Days post sorting
WT Control
WT CBL^ΔE8/9RUNX1^S291fs
Asc-/- Control
Asc-/- CBL^ΔE8/9RUNX1^S291fs
n.s.
**
E
Culture
8 days
Lin- GFP+ hNGFR+ cells
Inflammasome stimulation
LPS (200 ng/mL, 4 h)
Nigericin (10 μM, 1 h)
Annexin V assay
ELISA
F
Control
CBL^ΔE8/9RUNX1^S291fs
No stimulation
Stimulation (LPS + Nigericin)
WT
Asc-/-
PI
Annexin V
0.066
13.8
55.6
30.6
0.27
42.3
27.5
29.8
0.039
9.57
65.1
25.3
0.17
34.8
33.2
31.8
0.13
27.5
32.1
42.1
0.028
56.3
19.2
24.5
0.19
12.2
56.2
31.4
0.082
43.0
28.8
28.1
G
No stimulation
LPS + Nigericin
Annexin V+PI- (%)
Annexin V+PI+ (%)
Ctr
CR
WT
Asc-/-
Annexin V+PI-
Annexin V+PI+
H
IL-1β
TNFα
IL-1β (×10^3 pg/ml)
TNFα (×10^3 pg/ml)
N.D.
n.s.
****

Figure 3

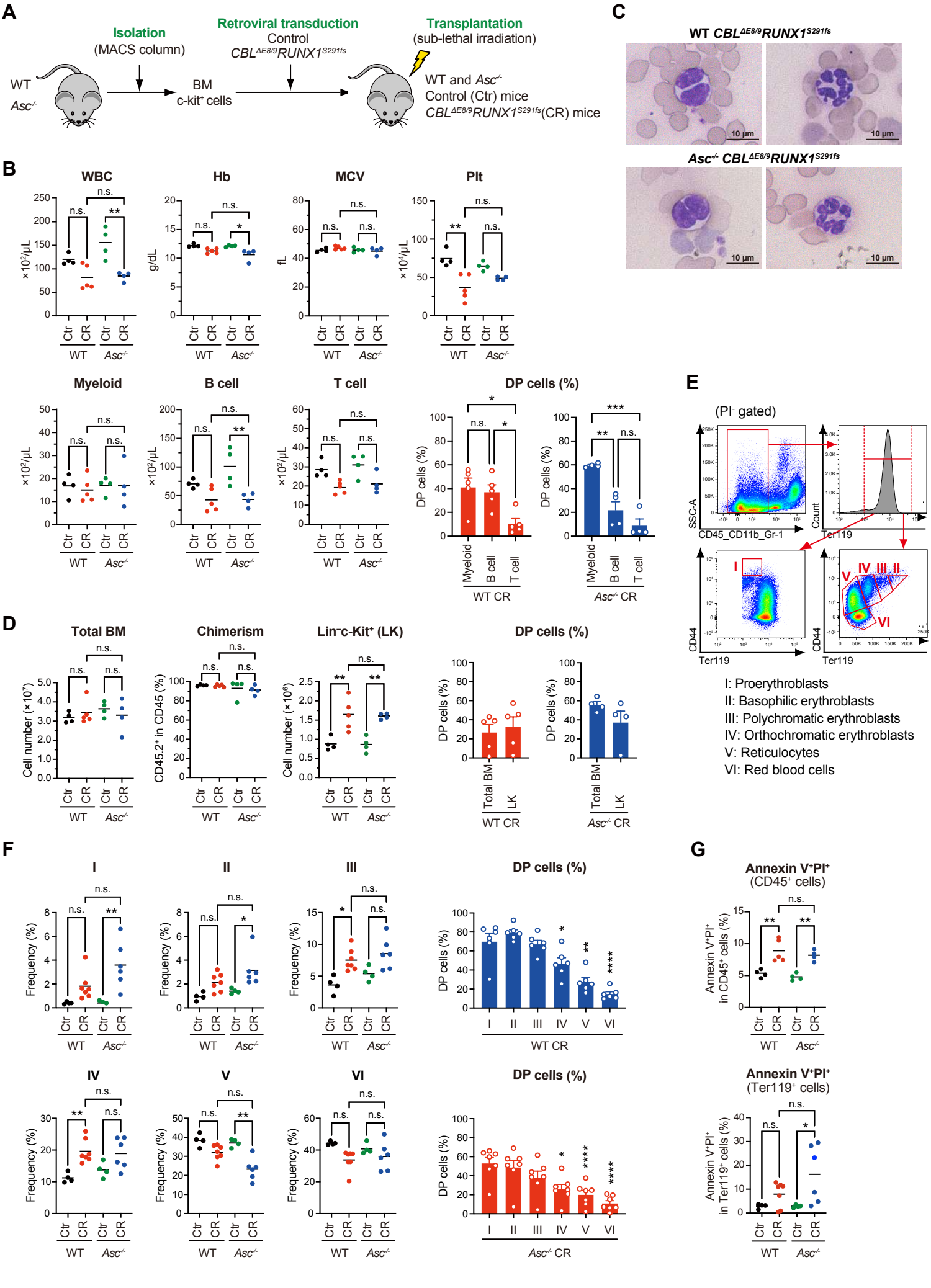
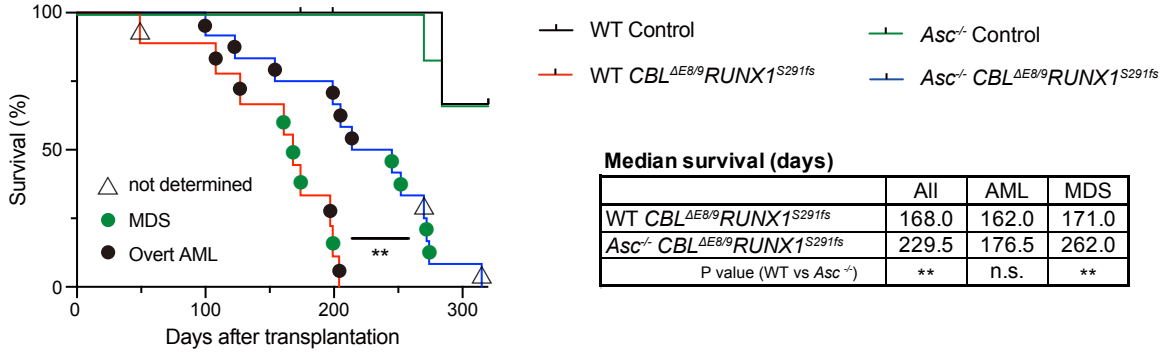

A
Isolation
(MACS column)
Retroviral transduction
Control
CBL^ΔE8/9RUNX1^S291fs
Transplantation
(sub-lethal irradiation)
WT
Asc-/-
BM
c-kit+ cells
WT and Asc-/-
Control (Ctr) mice
CBL^ΔE8/9RUNX1^S291fs (CR) mice
B
WBC
Hb
MCV
Plt
Myeloid
B cell
T cell
DP cells (%)
C
WT CBL^ΔE8/9RUNX1^S291fs
Asc-/- CBL^ΔE8/9RUNX1^S291fs
10 µm
D
Total BM
Chimerism
Lin-c-Kit+ (LK)
DP cells (%)
E
(PI- gated)
SSC-A
CD45_CD11b_Gr-1
Count
Ter119
CD44
I: Proerythroblasts
II: Basophilic erythroblasts
III: Polychromatic erythroblasts
IV: Orthochromatic erythroblasts
V: Reticulocytes
VI: Red blood cells
F
I
II
III
IV
V
VI
DP cells (%)
G
Annexin V+PI+ (CD45+ cells)
Annexin V+PI+ (Ter119+ cells)
WT
Asc-/-
Ctr
CR

Figure 4

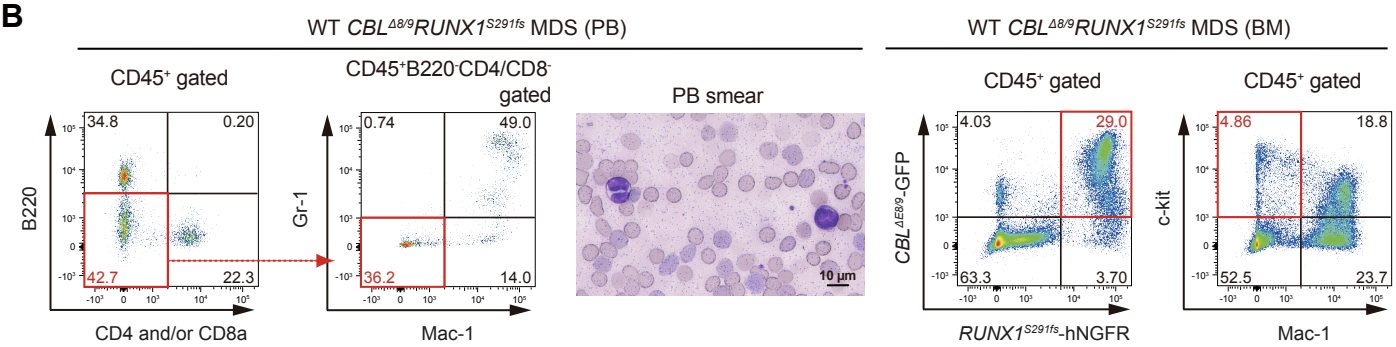
A



Median survival (days)

	All	AML	MDS
WT *CBL*$^{\Delta E8/9}$*RUNX1*^{S291fs}	168.0	162.0	171.0
Asc$^{-/-}$ *CBL*$^{\Delta E8/9}$*RUNX1*^{S291fs}	229.5	176.5	262.0
P value (WT vs *Asc* $^{-/-}$)	**	n.s.	**

B



C

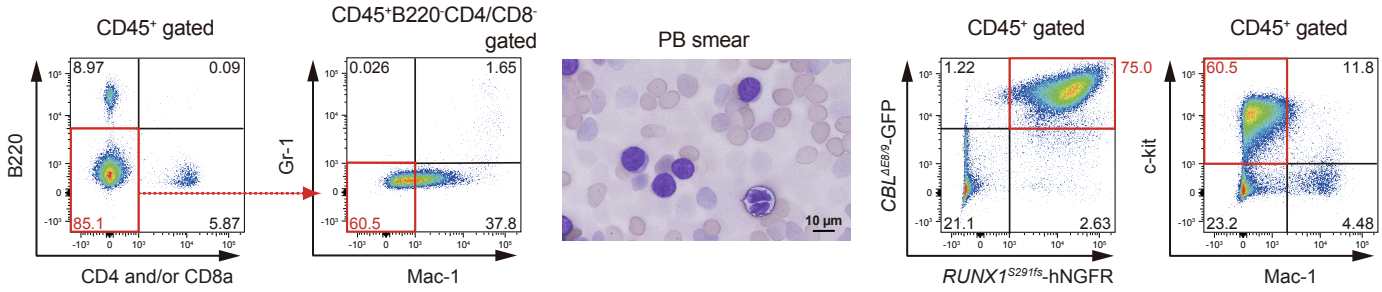


Figure 5

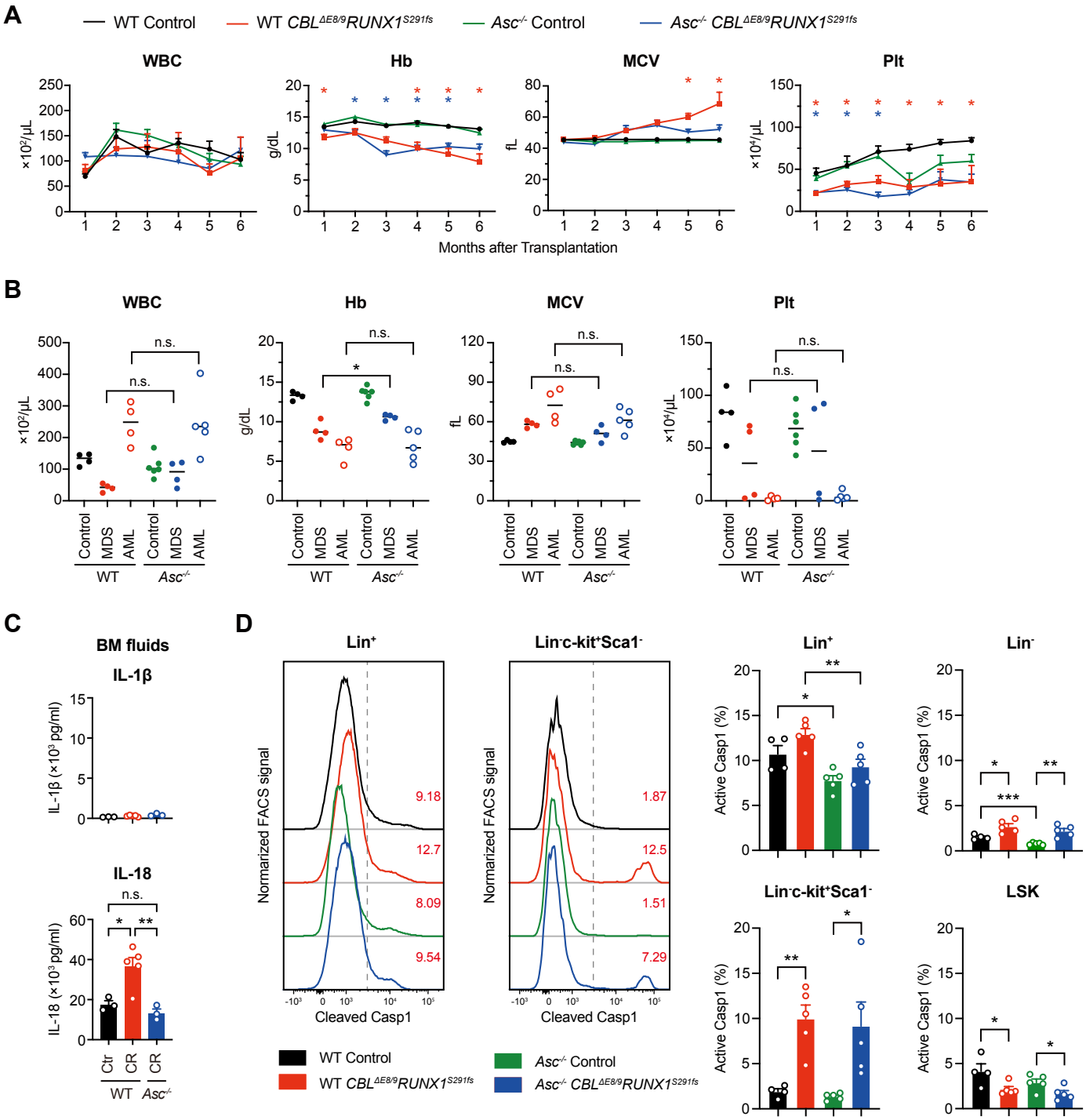
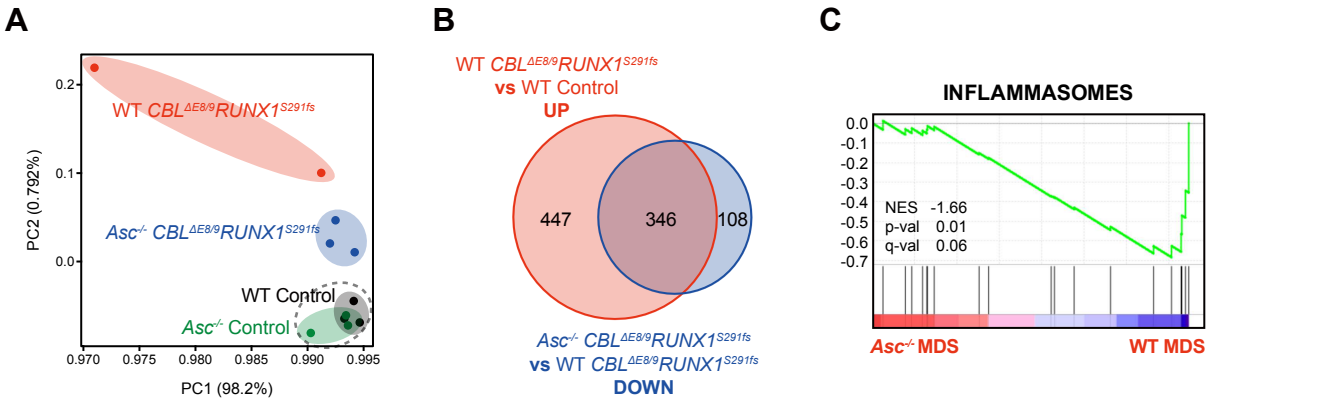
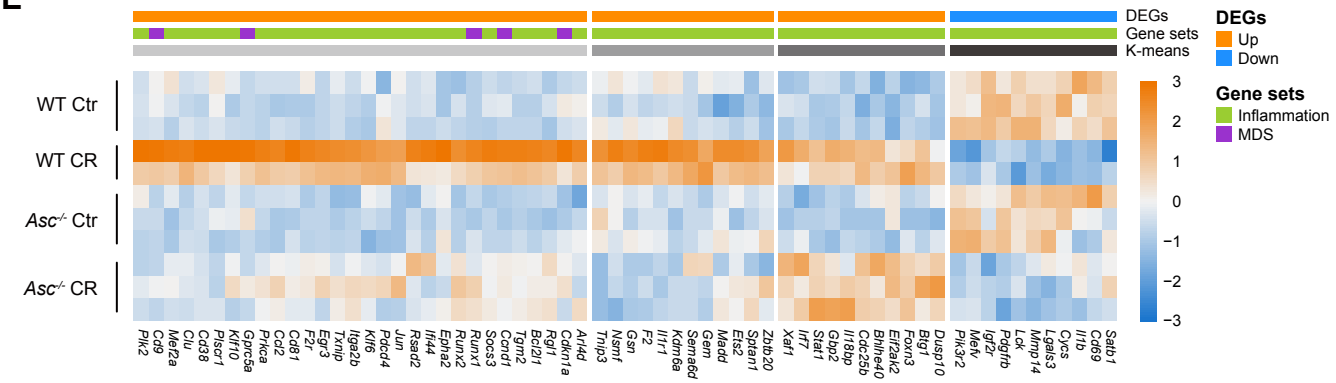

A
WT Control
WT CBL^ΔE8/9 RUNX1^S291fs
Asc-/- Control
Asc-/- CBL^ΔE8/9 RUNX1^S291fs
WBC
Hb
MCV
Plt
Months after Transplantation
B
WBC
Hb
MCV
Plt
n.s.
Control
MDS
AML
WT
Asc-/-
C
BM fluids
IL-1β
IL-1β (×10³ pg/ml)
IL-18
IL-18 (×10³ pg/ml)
Ctr
CR
WT
Asc-/-
D
Lin+
Lin-c-kit+Sca1-
Normarized FACS signal
Cleaved Casp1
9.18
12.7
8.09
9.54
1.87
12.5
1.51
7.29
WT Control
WT CBL^ΔE8/9 RUNX1^S291fs
Asc-/- Control
Asc-/- CBL^ΔE8/9 RUNX1^S291fs
Lin-
LSK
Active Casp1 (%)

Figure 6



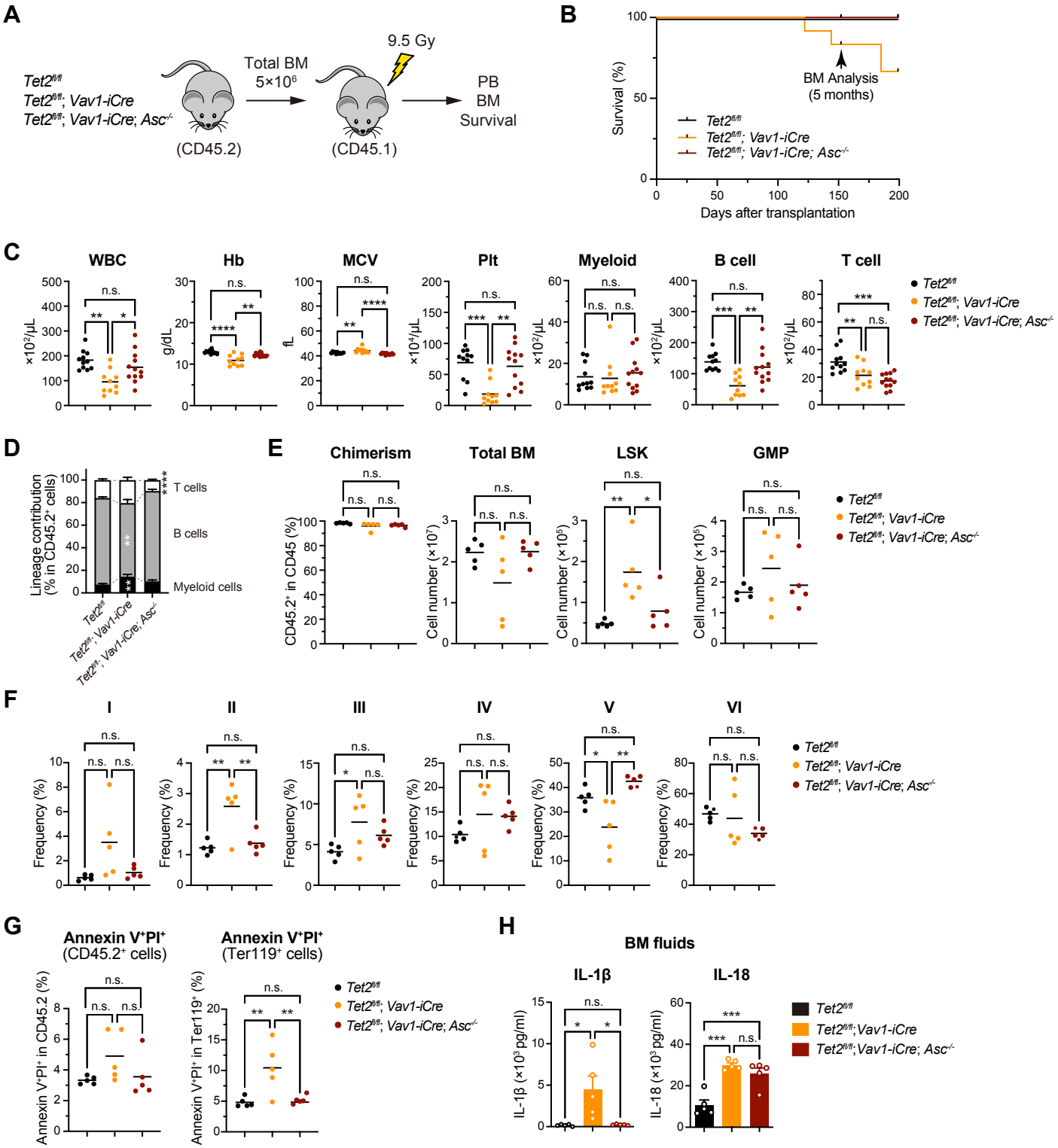
D

Gene set		WT MDS vs. WT control			Asc-/- MDS vs. WT MDS		
		NES	p-val	q-val	NES	p-val	q-val
Inflammation	INFLAMMASOMES	1.10	0.35	0.47	-1.66	0.01	0.06
	IL1_SIGNALING	1.34	0.06	0.20	-0.74	0.86	0.93
	IL18_SIGNALING	1.51	0.00	0.10	-1.40	0.01	0.21
	TNF_TARGETS_UP	1.92	0.00	0.01	-1.60	0.01	0.08
	INTERFERON_RESPONSIVE_GENES	1.89	0.00	0.01	-0.90	0.64	0.79
	APOPTOSIS	1.36	0.03	0.07	-1.41	0.02	0.06
MDS	MYELODYSPLASTIC_SYNDROM_RISK_UP	1.35	0.12	0.19	-1.38	0.12	0.22
	MYELODYSPLASTIC_SYNDROM_LOW_RISK_UP	1.42	0.09	0.14	-1.26	0.20	0.34
Cell growth / Protein systhesis	MYC_TARGETS_UP	-2.54	0.00	0.00	2.39	0.00	0.00
	G2_M_CHECKPOINTS	-1.76	0.00	0.02	1.95	0.00	0.01
	DNA_REPLICATION	-2.43	0.00	0.00	2.33	0.00	0.00
	RIBOSOME	-3.33	0.00	0.00	3.04	0.00	0.00
	EUKARYOTIC_TRANSLATION_ELONGATION	-3.39	0.00	0.00	3.07	0.00	0.00
	EUKARYOTIC_TRANSLATION_INITIATION	-3.23	0.00	0.00	2.98	0.00	0.00



E

Figure 7


A
Tet2fl/fl
Tet2fl/fl; Vav1-iCre
Tet2fl/fl; Vav1-iCre; Asc-/-
Total BM
5×10⁶
9.5 Gy
(CD45.2)
(CD45.1)
PB
BM
Survival
B
Survival (%)
BM Analysis
(5 months)
Days after transplantation
C
WBC
Hb
MCV
Plt
Myeloid
B cell
T cell
D
Lineage contribution
(% in CD45.2+ cells)
T cells
B cells
Myeloid cells
E
Chimerism
Total BM
LSK
GMP
CD45.2+ in CD45 (%)
Cell number (×10⁷)
Cell number (×10⁵)
F
I
II
III
IV
V
VI
Frequency (%)
G
Annexin V+PI+
(CD45.2+ cells)
Annexin V+PI+
(Ter119+ cells)
Annexin V+PI+ in CD45.2 (%)
Annexin V+PI+ in Ter119+ (%)
H
BM fluids
IL-1β
IL-18
IL-1β (×10³ pg/ml)
IL-18 (×10³ pg/ml)

Supplementary Files

This is a list of supplementary files associated with this preprint. Click to download.

- SupplementaryTable12.xlsx
- ResponsetoRefereescomment20260818.pdf
- SupplementaryInformation.pdf